Supplementary Material

Well-controlled Three-dimensional Tree-like Core-shell Structural Electrode for Flexible All-solid-state Supercapacitors with Favorable Mechanical and Electrochemical Durability

Hao Gu[a], Yiqing Zeng[a], Shipeng Wan[a], Shule Zhang[a], Qin Zhong[a]*, Yunfei Bu[b]**

[a] School of Chemical Engineering, Nanjing University of Science and Technology, Nanjing 210094, PR China

[b] Jiangsu Collaborative Innovation Center of Atmospheric Environment and Equipment Technology (CICAEET), Jiangsu Key Laboratory of Atmospheric Environment Monitoring and Pollution Control (AEMPC), UNIST-NUIST Research Center of Environment and Energy (UNNU), School of Environment Science and Engineering, Nanjing University of Information Science and Technology, Nanjing 210044, PR China

*Corresponding author. E-mail address: zq304@njust.edu.cn (Q. Zhong),

**Corresponding author. E-mail address: yunfei.bu@nuist.edu.cn (Y. Bu)

1. Electrochemical reaction equations.

CV curves exhibited the charge storage of the outer NCCH shell can be ascribed to the redox reactions as the following equations:

$$Ni(OH)_2 + OH^- \leftrightarrow NiOOH + e^- \quad (1)$$

$$Co(OH)_2 + OH^- \leftrightarrow CoOOH + e^- \quad (2)$$

$$CoOOH + OH^- \leftrightarrow CoO_2 + H_2O + e^- \quad (3)$$

The redox reaction of the inner NS core can be shown as follow:

$$NiSe_2 + OH^- \leftrightarrow NiSe_2OH + e^- \quad (4)$$

2. Experimental Part.

2.1 Chemicals

All analytical grade chemical reagents were used in experiments without further purification. Nickel foam (NF) was provided by Changs ha Liyuan New Materials Co., Ltd. Hydrochloric acid (HCl), nitric acid (HNO_3) was purchased from Beijing Chemical Works. $Ni(NO_3)_2{\cdot}6H_2O$, $Co(NO_3)_2{\cdot}6H_2O$ were purchased from Guangdong Chemical Reagent Engineering Rapid Research and Development Center. Active carbon (AC) was bought from Shanghai Keleli Co., Ltd. Other reagents were obtained from Aladdin. The water used in all experiments was purified through a Millipore system.

2.2 Fabrication of Ni-plated carbon cloth (NPCC)

The electroless plating process was utilized for the fabrication of Ni-plated carbon cloth. Firstly, a piece of carbon cloth (1 cm × 2 cm) was sonicated for 30 minutes in acetone, ethanol and deionized water successively, and then dried overnight. The clean carbon cloth needed a pretreatment process before immersed in an electroless plating bath. The carbon cloth was soaked in an etching solution (composed of concentrated HNO_3), a sensitizing solution (composed of 20g/L $SnCl_2{\cdot}2H_2O$ and 40 mL/L HCl) and an activation solution (composed of 0.25 g/L $PbCl_2$ and 2.5 mL/L HCl) for 30 minutes successively. Finally, the treated carbon cloth was immersed in an electroless plating bath (composed of 0.12 mol/L nickel acetate, 0.016 mol/L Na_2EDTA, 0.15 mol/L lactic

acid, 7.5 g/L NaOH and 0.4 mol/L hydrazine hydrate) for 30 minutes in 75 °C. The Ni-plated carbon cloth (NPCC) was obtained after washing and drying.

2.3 Fabrication of NiSe/Ni-plated carbon cloth (NS/NPCC)

NiSe nanorod arrays were grown in situ on NPCC via an improved solvothermal method. In a 5 mL tube, 19.74 mg selenium powder, 18.92 mg $NaBH_4$ and 1 mL anhydrous ethanol were added successively to obtain a transparent NaSeH ethanol solution. The solution was quickly poured into a 50 mL Teflon-lined stainless-steel autoclave containing 20 mL anhydrous ethanol and a piece of NPCC (1 cm × 2 cm) under N_2 flow. Then the autoclave was sealed and heated at 160 °C for 12 h. The NiSe/Ni-plated carbon cloth (NS/NPCC) was obtained after washing using ethanol and drying at 60 °C overnight.

2.4 Fabrication of NiSe@NiCo$(CO_3)(OH)_2$/Ni-plated carbon cloth (NS@NCCH/NPCC)

Two-dimensional $NiCo(CO_3)(OH)_2$ nanosheets were anchored on the NiSe nanorod arrays via a facile hydrothermal process. $Co(NO_3)_2 \cdot 6H_2O$ (0.11 M), $Ni(NO_3)_2 \cdot 6H_2O$ (40 mM) and urea (1.15 M) were dissolved in 20 mL deionized water. Then, the obtained precursor solution and a piece of as-prepared NS/NPCC (1 cm × 2 cm) were added into a 50 mL Teflon-lined stainless-steel autoclave and kept in an oven at 85 °C for 2 h. The $NiCo(CO_3)(OH)_2$@NiSe/Ni-plated carbon cloth (NS@NCCH/NPCC) electrode was obtained after washing and drying at 60 °C overnight.

For comparison, four electrodes, involving NiSe@$Co_2(CO_3)(OH)_2$/Ni-plated carbon cloth (NS@CCH/NPCC), NiSe/Ni-plated carbon cloth (NS/NPCC), $NiCo(CO_3)(OH)_2$/Ni-plated carbon cloth (NCCH/NPCC) and NiSe@$NiCo(CO_3)(OH)_2$/nickel foam (NS@NCCH/NF) were also prepared in a similar procedure.

3. Materials characterizations

The crystal structure was characterized by Powder X-ray diffraction (XRD, Beijing Purkinjie general instrument XD-3, Cu Kα radiation) and Fourier transform

infrared (FT-IR, Nicolet iS-10). The composition and morphology of NS@NCCH/NPCC were investigated by field emission scanning electron microscope (FE-SEM, Quaint 250FEG) with an energy dispersive X-ray spectroscopy (EDS) and high-resolution transmission electron microscope (HRTEM, JEOLJEM 2100).

4. The method of assembly flexible all-solid-state asymmetric supercapacitor (NS@NCCH/NPCC//AC/CC)

A flexible all-solid-state asymmetric supercapacitor (FASSAS) device was assembled by an activated carbon/carbon cloth (AC/CC) negative electrode and a NS@NCCH/NPCC positive electrode with a KOH/PVA gel electrolyte. The AC/CC negative electrode was prepared by spraying slurry consisting of activated carbon (AC, 90 %) and polyvinylidene fluoride (PVDF, 10 %) on the carbon cloth. The KOH/PVA gel electrolyte was prepared by a typical process. Specifically, 6 g of PVA was dispersed in 40 mL of deionized water at 95 °C to form a homogeneous solution. After the solution was cooled to about 50 °C, the KOH solution (3 g KOH dissolved in 20 mL deionized water) was added dropwise under vigorous stirring to obtain the KOH/PVA gel electrolyte. After the preparation of the gel electrolyte, a robust FASSAS was prepared by pairing NS@NCCH/NPCC and AC/CC electrodes covered with KOH/PVA gel electrolyte face to face. Then the device was sealed for electrochemical characterization.

5. Illustration for the reaction mechanism in the fabrication process of NS@NCCH/NPCC

Hierarchical three dimensional NS@NCCH/NPCC flexible electrode was obtained via three-step progress as illustrated in Fig. 1a. Ni-plated carbon cloth (NPCC), as a substrate to grow the electroactive material and a source of nickel in the fabrication process, was firstly fabricated through a electroless plating process. In the electroless plating solution, Ni^{2+} species, adsorbed on the surface of carbon cloth, were reduced by hydrazine hydrate under the several additives condition, to form uniform Ni coating layer. Then, one-dimensional NS nanorod arrays grow in situ on the surface of NPCC utilizing NPCC as a nickel source and NaHSe as a selenium source. NaHSe

ethanol solution was prior prepared, as show in the following reaction [1]:

$$2NaBH_4 + 2Se \xrightarrow{EtOH} 2NaHSe + 3H_2\uparrow \quad (5)$$

To build a hierarchical three-dimensional structure, two-dimensional NCCH nanosheets were anchoring on the one-dimensional NS nanorod arrays via a solvothermal reaction, based on the heterogeneous nucleation and growth reaction [2]. Urea decomposed at high temperature and pressure, providing hydrogen and carbonate for the generation of nuclei of metal carbonate hydroxides. To reduce the surface energy of 1D NS nanorod arrays, Ni^{2+} and Co^{2+} condensed on the surface of NS nanorod arrays and generated nuclei of NCCH. Thereafter, the NCCH nuclei were continuously grown along the crystal nuclei to form the 2D NCCH nanosheets. The following equation shows the whole reaction process [3]:

$$2CO(NH_2)_2 + 3H_2O \rightarrow 2NH_4^+ + 2OH^- + CO_2 \quad (6)$$

$$2OH^- + CO_2 \rightarrow H_2O + CO_3^{2-} \quad (7)$$

$$Ni^{2+} + Co^{2+} + CO_3^{2-} + 2OH^- \rightarrow NiCo(CO_3)(OH)_2 \quad (8)$$

6. Electrochemical measurement

The electrochemical performance, including the cycle voltammeter (CV), galvanostatic charge-discharge (GCD) and electrochemical impedance spectroscopy (EIS) was tested on an electrochemical workstation (IVIUMnSTAT) by a traditional three-electrode system. The prepared electrodes, platinum foil and Hg/HgO electrode were used as the work, counter and reference electrodes, respectively. In addition, the cycle stability was evaluated by a CT2001A LAND Cell test system.

The areal specific capacitance (C, mF cm^{-2}) was calculated by the following Eq. (9):

$$C = \frac{I\Delta t}{s\Delta V} \quad (9)$$

where I (mA) is the discharge current, Δt (s) is the discharge time, ΔV (V) is the potential window, and s (cm^{-2}) is the area of the electrode.

The energy density E (Wh kg^{-1}) and power density P (W kg^{-1}) of the FASSASs

were calculated by the following Eq. (10) and (11):

$$E = \frac{C(\Delta V)^2}{2 \times 3600} \tag{10}$$

$$P = \frac{3600E}{\Delta t} \tag{11}$$

where C (F g^{-1}) is the calculated FASSASs capacitance, ΔV (V) and Δt (s) are the voltage range and the discharge time, respectively.

7. Supplementary figures

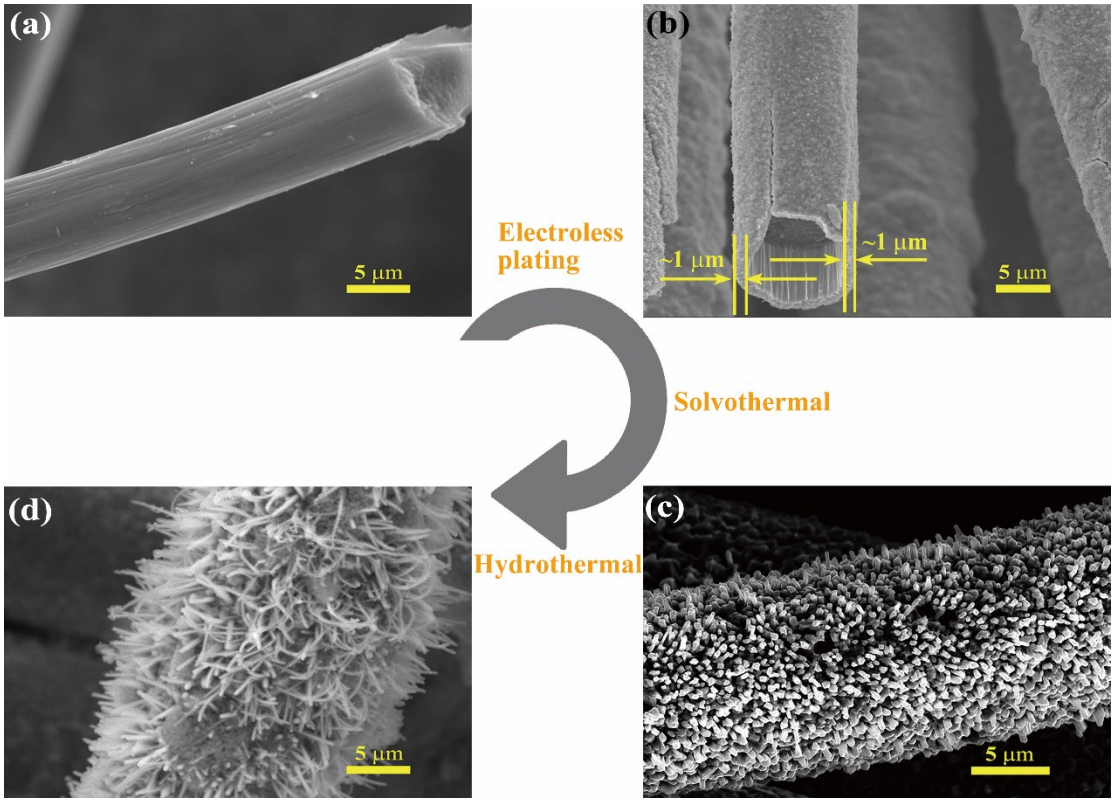

Fig. S1. SEM images of (a) CC, (b) NPCC, (c) NS/NPCC and (d) NS@NCCH/NPCC in the fabrication process.

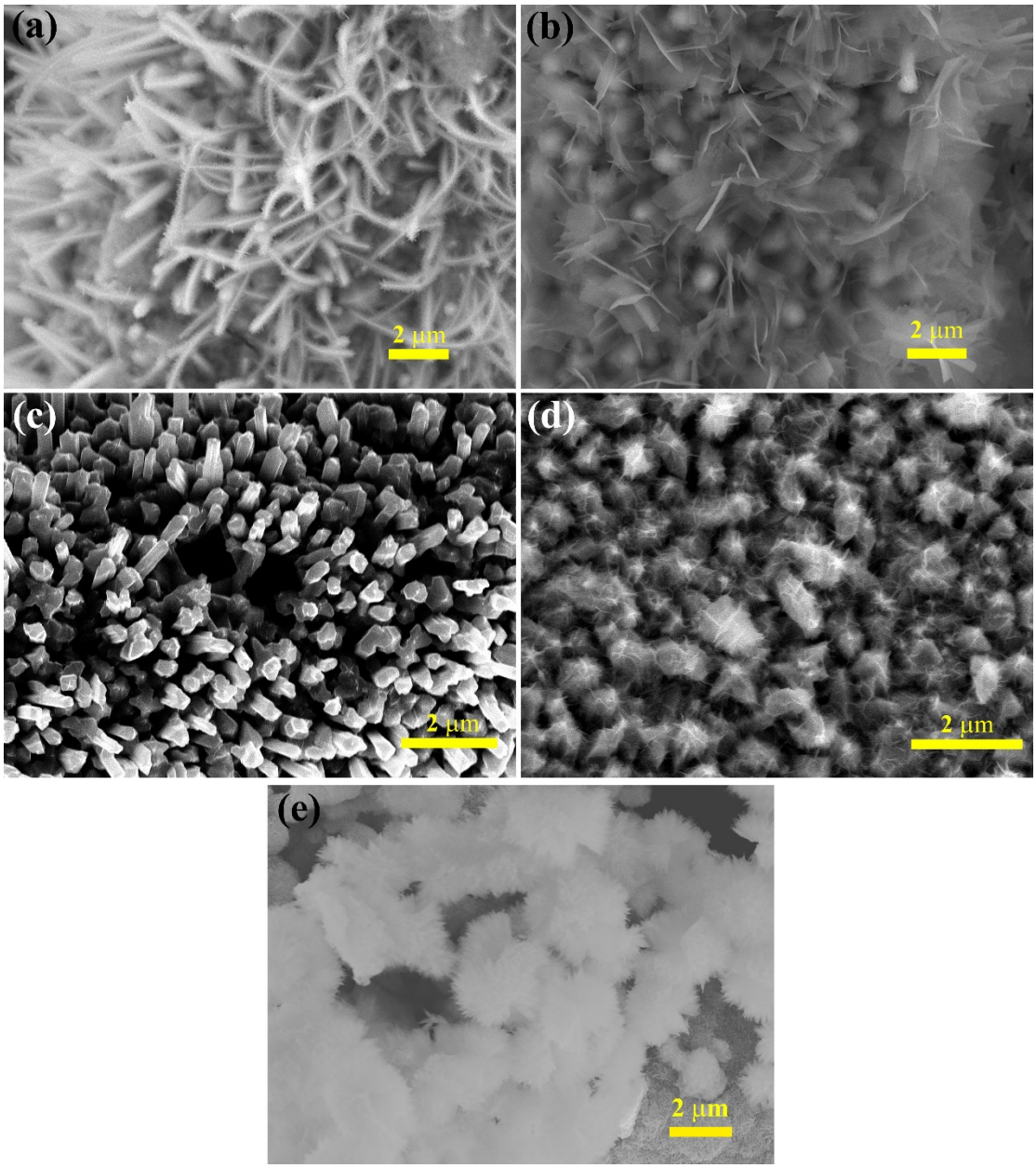

Fig. S2. SEM images of (a) NS@NCCH/NPCC, (b) NS@CCH/NPCC, (c) NS/NPCC, (d) NS@NCCH/NF and (e) NCCH/NPCC.

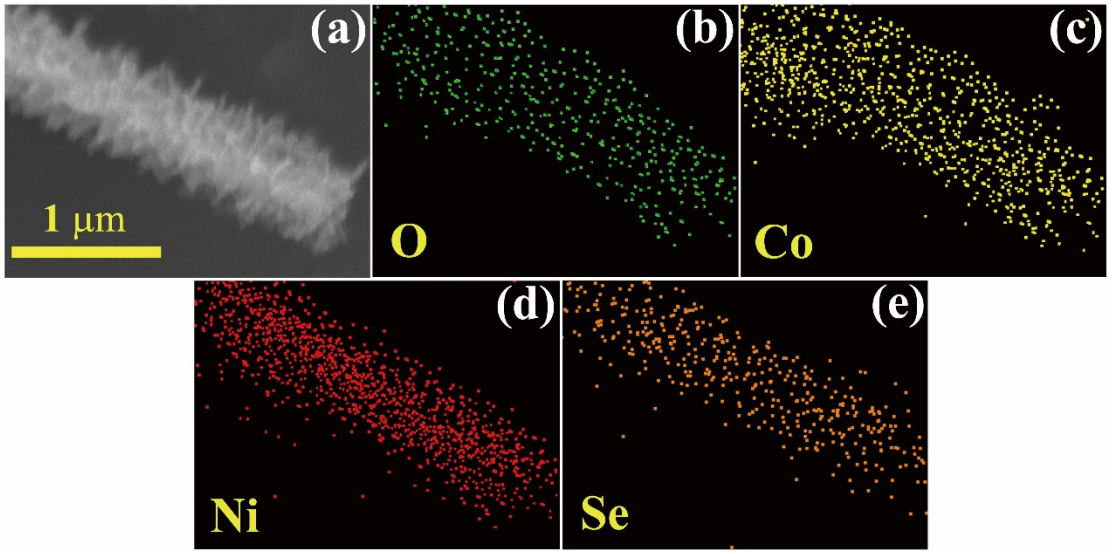

Fig. S3. (a) FESEM image of NS@NCCH and the corresponding EDS mapping for (b) O, (c) Co, (d) Ni and (e) Se.

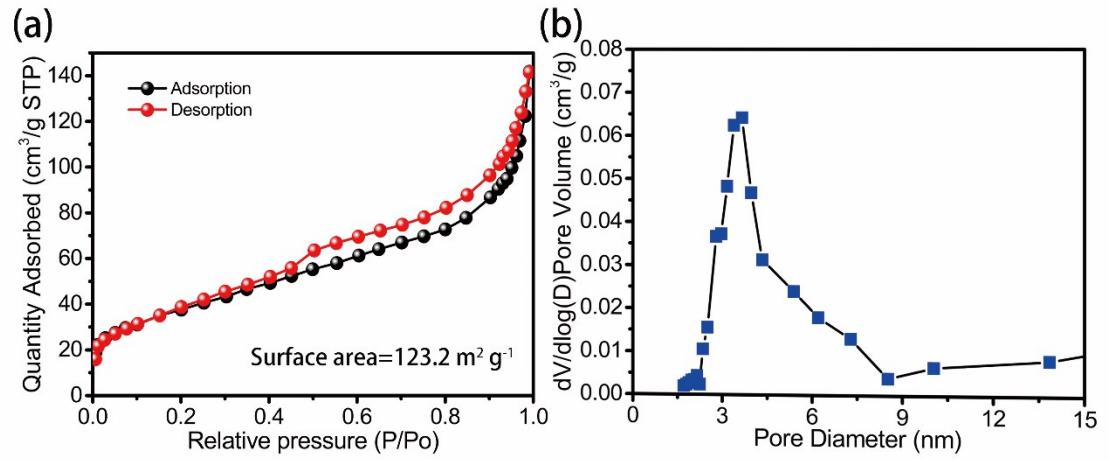

Fig. S4 (a) N_2 adsorption/desorption isotherm and (b) pore-size distribution of the NS@NCCH/NPCC.

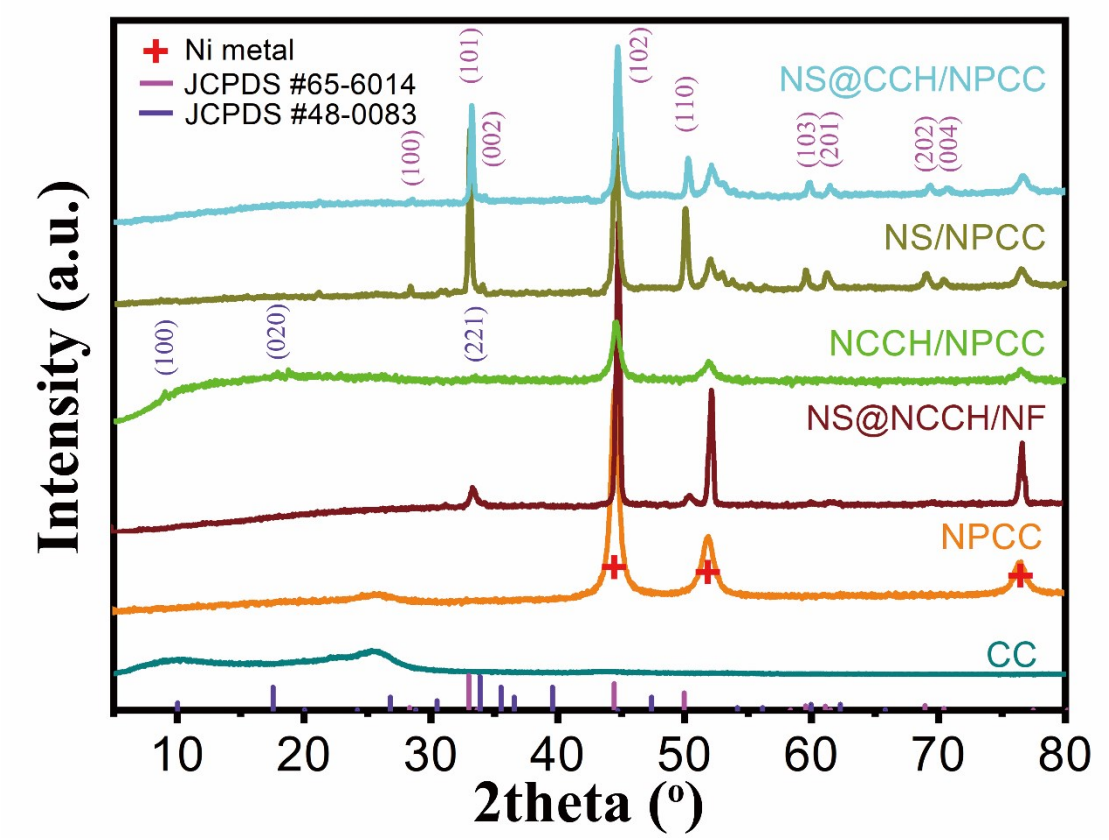

Fig. S5. XRD patterns of control samples, including NS@CCH/NPCC, NS/NPCC, NCCH/NPCC and NS@NCCH/NF.

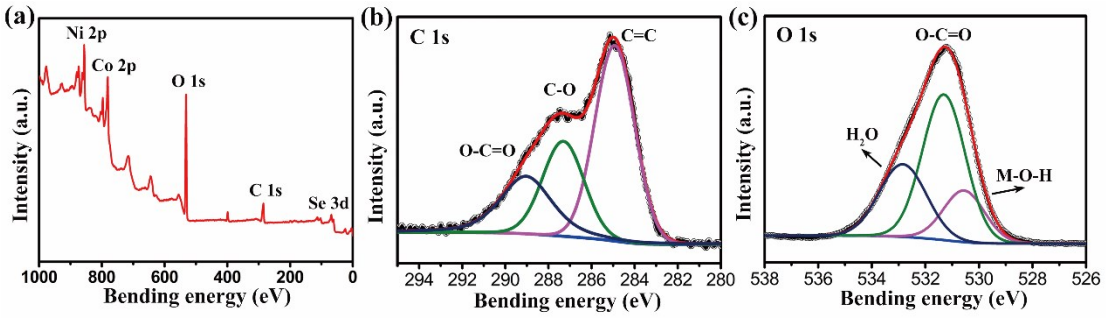

Fig. S6. XPS spectra of NS@NCCH/NPCC (a) full scan survey, (b) C 1s, (c) O 1s.

The composition of the synthesized NS@NCCH/NPCC was investigated by FT-IR in the range of 500-4000 cm^{-1}, with the results shown in Fig. S5. Two broad peaks at 3441 and 1615 cm^{-1} can be indexed to the stretching vibration and bending vibration of O-H, which are the features of water molecules and the carbonate hydroxide, respectively. The bands centered at 1355 and 1096 cm^{-1} arise from the asymmetrical and symmetrical stretching vibration of CO_3^{2-}. Additionally, two narrow peaks at 830 and 634 cm^{-1} are observed, corresponding to the in-plane and out-of-plane bending vibration of $CO_3^{2-,}$ respectively. This results clearly support the presence of the carbonate group and hydroxide group in the NS@NCCH/NPCC.

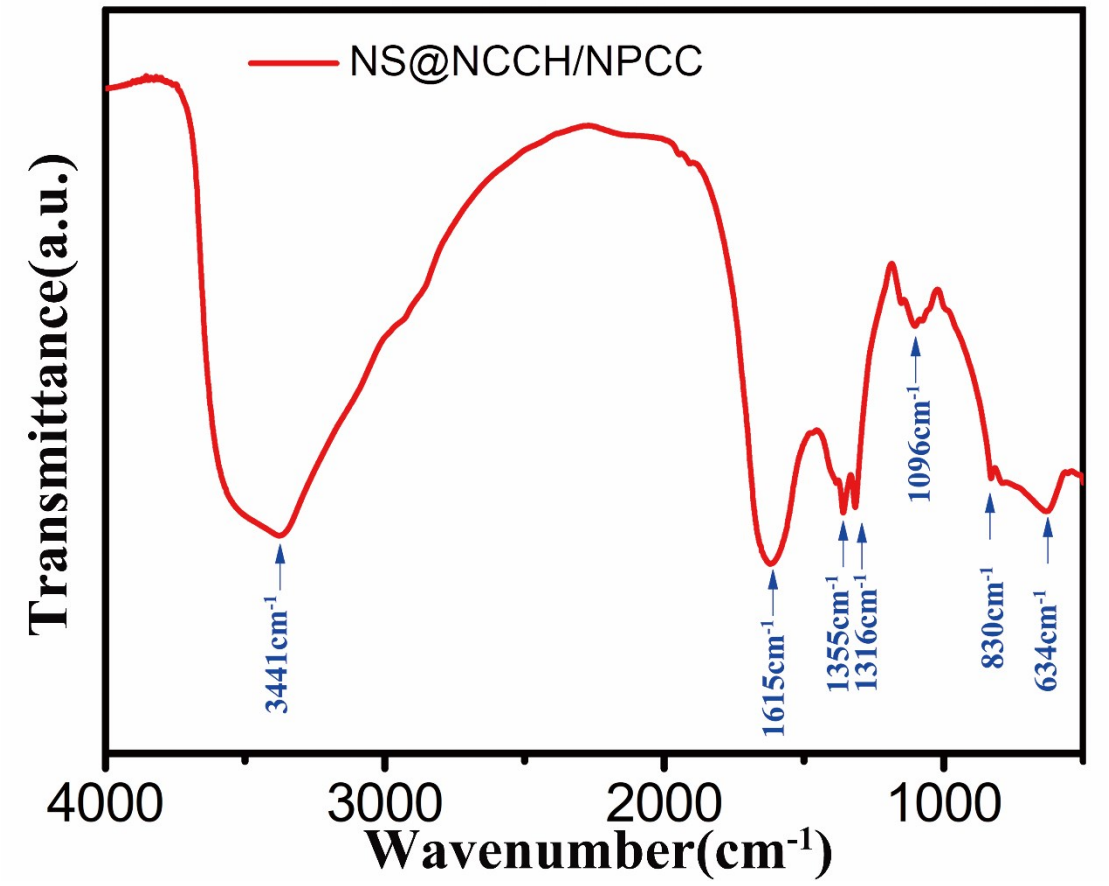

Fig. S7. FT-IR spectra of NS@NCCH/NPCC.

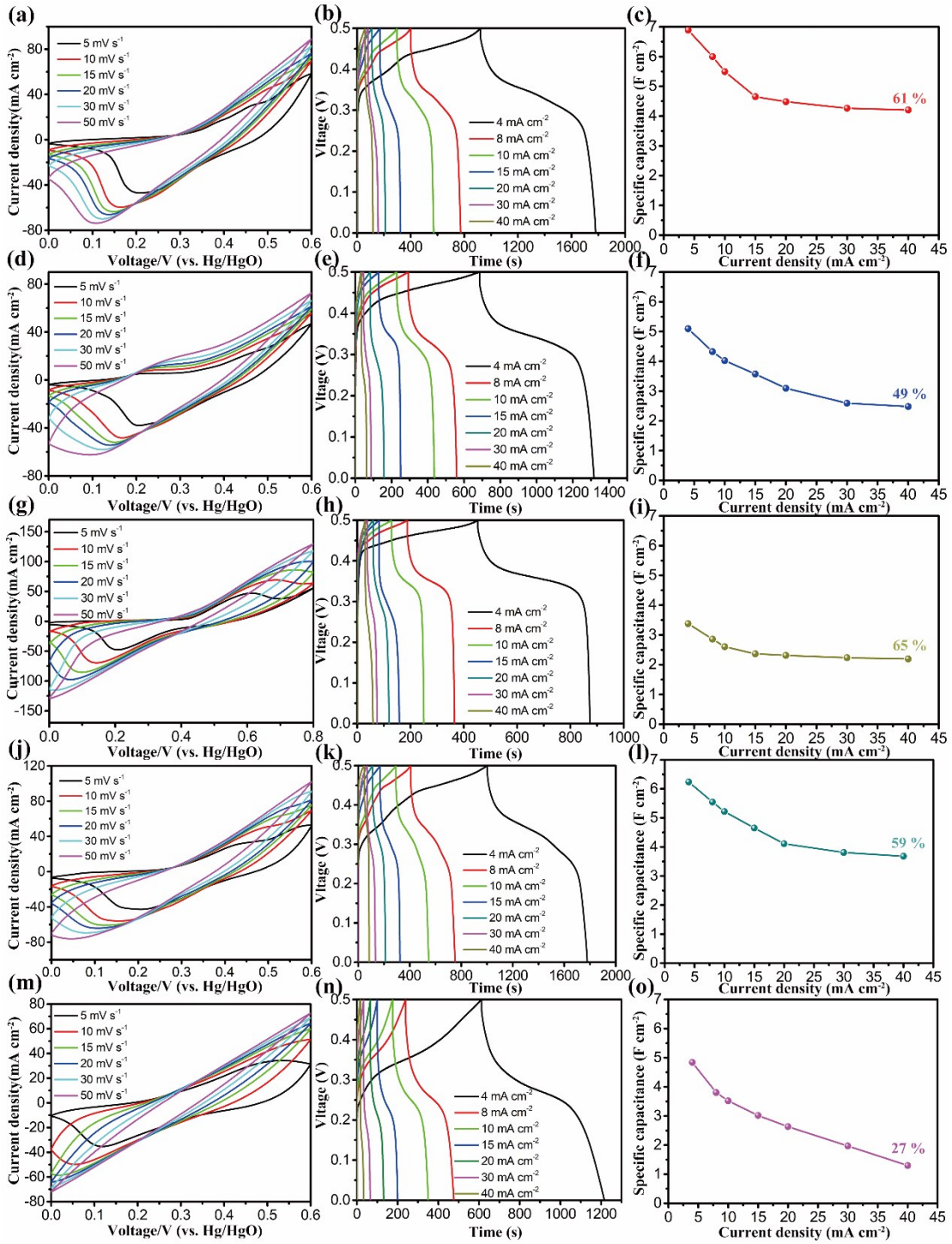

Fig. S8. Typical CV curves of (a) NS@NCCH/NPCC, (d) NS@CCH/NPCC, (g) NS/NPCC, (j) NS@NCCH/NF and (m) NCCH/NPCC at various scan rates ranging from 5 to 50 mV s^{-1}. GCD curves of (b) NS@NCCH/NPCC, (e) NS@CCH/NPCC, (h) NS/NPCC, (k) NS@NCCH/NF and (n) NCCH/NPCC at various current densities. Specific capacitances of (c) NS@NCCH/NPCC, (f) NS@CCH/NPCC, (i) NS/NPCC, (l) NS@NCCH/NF and (o) NCCH/NPCC at different current densities.

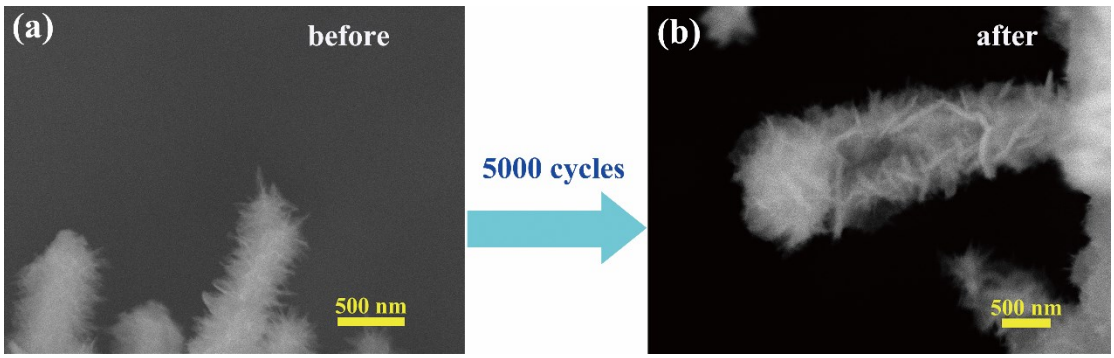

Fig. S9. SEM images of NS@NCCH/NPCC (a) before 5000 cycles test, (b) after 5000 cycles test.

In Fig. S10, NS@NCCH/NPCC electrodes are attached to the conductive glue under bending (180 °), rolling and twisting (180 °). However, NS@NCCH/NPCC fibers are merely slightly bent (less than 90 °) as seen in FESEM images of NS@NCCH/NPCC electrodes (Fig. S10b-d). Then, we bend a single NS@NCCH/NPCC fiber to 90 ° in Fig. S10e and f. On the surface of NS@NCCH/NPCC fiber, the bending has no effect on the structure of NS@NCCH/NPCC. The NS@NCCH core-shell microarrays does not shed off and no cracking or fracture appears.

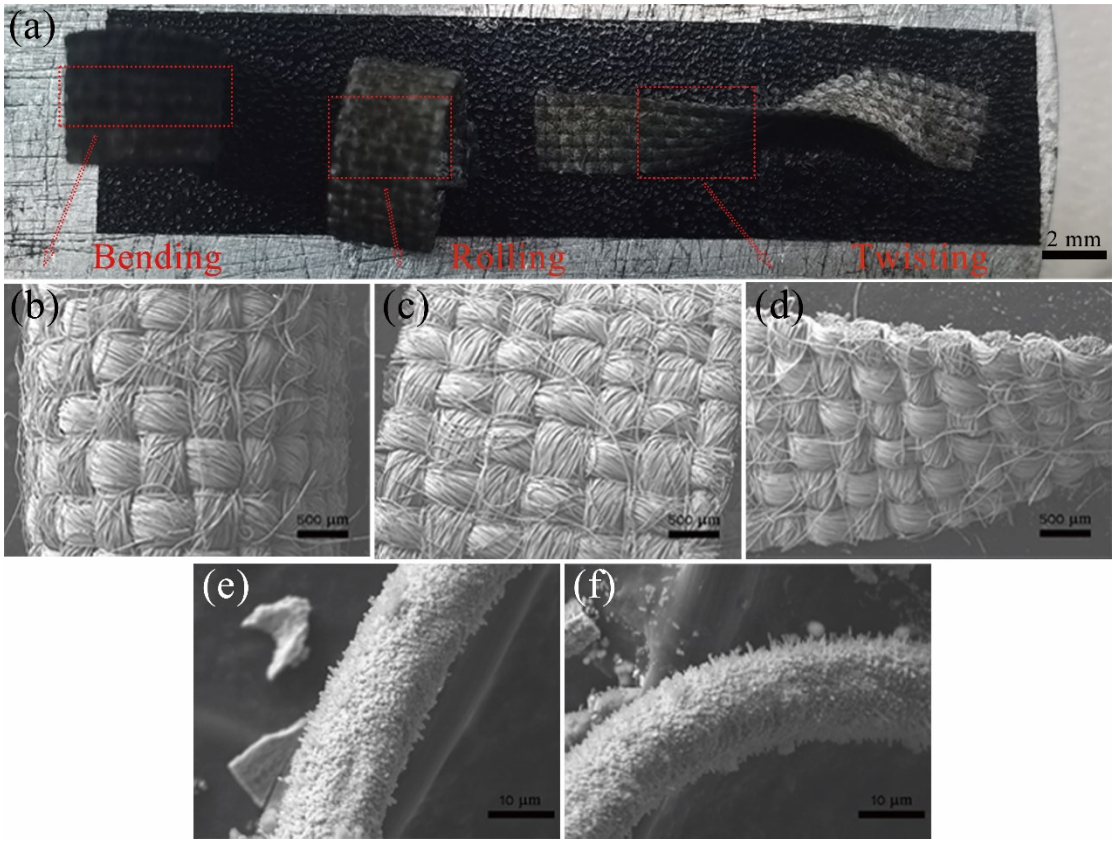

Fig. S10. (a) photograph of NS@NCCH/NPCC electrode under bending, rolling and twisting, FESEM images of NS@NCCH/NPCC electrode under bending (b), rolling (c) and twisting (d), FESEM images of a single NS@NCCH/NPCC fiber under normal (e) and bending (f).

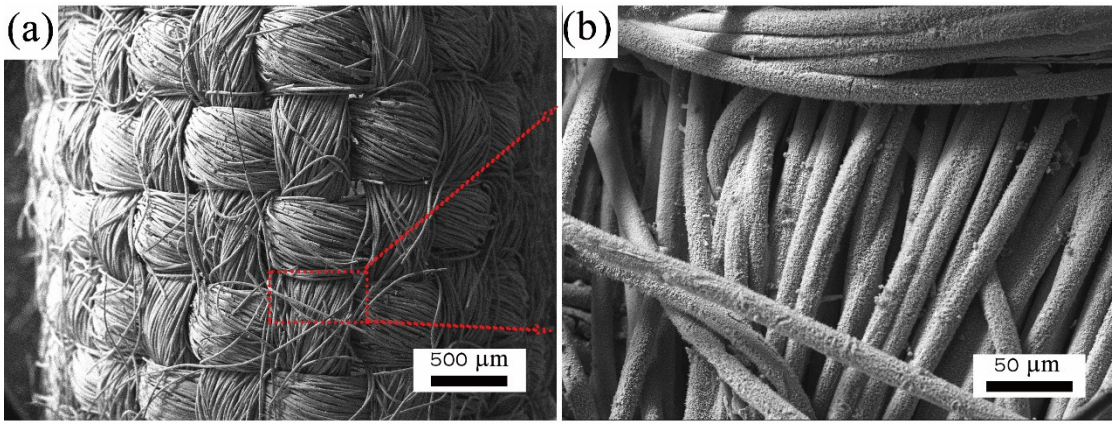

Fig. S11. FESEM images of NS@NCCH/NPCC electrode after 5000-time bending cycles (angle is 90 °).

Fig. S12. Two assembled FASSAS devices connected in series light up the red LED indicator for 6 minutes under (a) normal and (b) bending conditions.

Table 1 A comparison of difference materials and corresponding devices in terms of electrochemical performance

Material	Electrolyte	Capacitance	Corresponding device	Energy capacitance	Cycle stability	Reference
$(Ni,Co)Se_2$/NiCo-LDH	3 M KOH	1224 F g^{-1} at 2 A g^{-1}	$(Ni,Co)Se_2$/NiCo-LDH//porous carbon	39 Wh kg^{-1} at 1650 W kg^{-1}	89 % - 3000 cycles	4
$Ni_2P_2O_7$/NiCo-OH	2 M KOH	4.3 F cm^{-2} at 1 mA cm^{-2}	$Ni_2P_2O_7$/NiCo-OH//active carbon	78 Wh kg^{-1} at 444 W kg^{-1}	91.83 % - 10000 cycles	5
Ti_3C_2/Ni-Co-Al-LDH	1 M KOH	748.2 F g^{-1} at 1 A g^{-1}	Ti_3C_2/Ni-Co-Al-LDH//active carbon	45.8 Wh kg^{-1} at 346 W kg^{-1}	97.8 % - 10000 cycles	6
FeOF/$Ni(OH)_2$	3 M KOH	1452 F g^{-1} at 1 A g^{-1}	FeOF/$Ni(OH)_2$// active carbon	47.1 Wh kg^{-1} at 274 W kg^{-1}	84.4 % - 5000 cycles	7
P-$(Ni,Co)Se_2$	3 M KOH	6.04 F cm^{-2} at 2 mA cm^{-2}	P-$(Ni,Co)Se_2$//ZIF derived carbon	45.0 Wh kg^{-1} at 446.3 W kg^{-1}	85.2 % - 3000 cycles	8
ZnS-Ni_7S_6/$Ni(OH)_2$	--	--	ZnS-Ni_7S_6/$Ni(OH)_2$ //NSGNs	68.85 Wh kg^{-1} at 700.6 W kg^{-1}	91.79 % - 10000 cycles	9
Ni-Co LDH/CBD	6 M KOH	2115 F g^{-1} at 1 A g^{-1}	Ni-Co LDH /CBD//active carbon	57.5 Wh kg^{-1} at 0.9 kW kg^{-1}	80.9 % - 5000 cycles	10
$Ni(OH)_2$/graphene	6 M KOH	245 F g^{-1} at 1 A g^{-1}	$Ni(OH)_2$/graphene//porous graphene	77.8 Wh kg^{-1} at 174.7 W kg^{-1}	94.3 % - 3000 cycles	11
NS@NCCH/NPCC	1 M KOH	6.24 F cm^{-2} (1642 F g^{-1}, 228 mAh g^{-1}) at 4 mA cm^{-2}	NS@NCCH/NPCC// AC/CC	82.5 Wh kg^{-1} at 750 W kg^{-1}	91.5 % - 5000 cycles	This work

Video 1.mp4

Video 1. Two assembled FASSAS devices connected in series light up the red LED indicator for 6 minutes under normal or bending conditions (the video display was 6 times faster than the actual time of the experiment).

Reference:

1. C. Tang, N. Cheng, Z. Pu, W. Xing and X. Sun, *Angew Chem Int Ed Engl*, 2015, **54**, 9351-9355.
2. L. Mai, J. Sheng, L. Xu, S. Tan and J. Meng, *Acc Chem Res*, 2018, **51**, 950-959.
3. Z. Yu, Y. Chen, Z. Cheng, G. Tsekouras, X. Li, X. Wang, X. Kong and S. X. Dou, *Nano Energy*, 2018, **54**, 200-208.
4. X. Li, H. Wu, C. Guan, A. M. Elshahawy, Y. Dong, S. J. Pennycook and J. Wang, *Small*, 2019, **15**, 1803895-1803904.
5. N. R. Chodankar, D. P. Dubal, S. H. Ji and D. H. Kim, *Small*, 2019, **15**, 1901145-1901155.
6. R. Zhao, M. Wang, D. Zhao, H. Li, C. Wang and L. Yin, *ACS Energy Letters*, 2017, **3**, 132-140.
7. M. Wang, Z. Li, C. Wang, R. Zhao, C. Li, D. Guo, L. Zhang and L. Yin, *Advanced Functional Materials*, 2017, **27**, 1701014-1701023.
8. Q. Zong, Y. Zhu, Q. Wang, H. Yang, Q. Zhang, J. Zhan and W. Du, *Chemical Engineering Journal*, 2020, **392**, 123664-123673.
9. G. Saeed, P. Bandyopadhyay, S. Kumar, N. H. Kim and J. H. Lee, *ACS Appl Mater Interfaces*, 2020, **12**, 47377-47388.
10. J. Zhao, C. Ge, Z. Zhao, Q. Wu, M. Liu, M. Yan, L. Yang, X. Wang and Z. Hu, *Nano Energy*, 2020, **76**, 105026-105033.
11. W. Wang, Y. Lu, M. Zhao, R. Luo, Y. Yang, T. Peng, H. Yan, X. Liu and Y. Luo, *ACS Nano*, 2019, **13**, 12206-12218.